Electromechanical Design of a Body Weight Support System for a Therapeutic Robot for Rodent Studies

by

Michaëlle Ntala Mayalu

Submitted to the Department of Mechanical Engineering in Partial Fulfillment of Requirements for the Degree of

Bachelor of Science

at the

Massachusetts Institute of Technology

June 2010

Signature of Author....
Department of Mechanical Engineering
May 11, 2010

Certified by.....
Neville Hogan
Sun Jae Professor Mechanical Engineering
Professor Brain & Cognitive Science
Director Newman Lab
Thesis Supervisor

Accepted by.....
John H. Lienhard V
Collins Professor of Mechanical Engineering
Chairman, Undergraduate Thesis Committee

Electromechanical Design of a Body Weight Support System for a Therapeutic Robot for Rodent Studies

By

Michaëlle Ntala Mayalu

Submitted to the Department of Mechanical Engineering
on May 11, 2010 in partial Fulfillment of the
Requirements of the Degree of Bachelor of Science in
Mechanical Engineering

ABSTRACT

As part of an ongoing effort to better understand and treat locomotor disorders, an over-ground therapeutic robot prototype to study recovery of locomotion after spinal cord injury in rodents is under development. One key element of the therapeutic robot is a system to support the partial body weight of a freely-moving rodent. This paper discusses the design requirements, fabrication, modeling, calibration and preliminary analysis of a highly back-drivable body-weight support system prototype. In addition, a closed loop feedback control system was designed, simulated, constructed and tested. Hardware limitations were identified, and alternative control techniques were explored.

Thesis Supervisor: Neville Hogan

Title: Prof. Mechanical Engineering; Prof Brain & Cog Science; Dir Newman Lab

Table of Contents

List of Figures

List of Appendices

Nomenclature

τ	actuation torque($N \cdot m$)
f	actuation the force(N)
J_{Tot}	moment of inertia due the rotating components in the system ($kg \cdot m^2$)
z	translational position along the arm(m)
θ	rotational position of the arm(rad)
ω, $\Omega(s)$	angular velocity of arm(rad/s)
α_{arm}	angular acceleration of arm(rad/s)
α_{rat}	angular acceleration of rat(rad/s)
i	motor current(A)
K_t ,K_e	Motor constant($V \cdot s/rad$, $N \cdot m/A$)
τ_i	internal torque of the motor ($N \cdot m$)
$U(s)$	input voltage to motor (V)
R	motor resistance (Ohms)
L	motor inductance (Farads)
b	constant relating angular velocity to friction force(damping constant) ($N \cdot m \cdot s/rad$)
τ_f	frictional torque ($N \cdot m$)
τ_m	mechanical time constant (s)
τ_e	electrical time constant (s)
l	length of the string between the rod and the Rat Module(m)
ϕ	angle that string is misaligned from the vertical (rad)
N	contact force between the rat and the ground (N)
N'	modified contact force when string is misaligned from the vertical (N)
W	weight of rat and Rat Module (N)
k	spring constant(N/m)
Δx	length change of the spring (m)
$A_{1,2}$	accelerometers
$R_{1,2}$	resistors
$C_{1,2}$	capacitors
K_{sen}	accelerometer sensor gain($V \cdot s/rad$)
V_{A1}	accelerometer voltage(V)

V_{supply} power supply voltage(V)

V_{LPF} accelerometer voltage after low pass filter(V)

K_p proportional controller gain

K_d derivative controller gains

ζ damping coefficient

1. Introduction

Recent applications of robotics to rehabilitation have enabled research on the recovery of lower extremity function after stroke or spinal cord injury (SCI) [1-6]. Spinal cord injury is a neurological disorder that results in the loss of motor and sensory function. This disorder can occur from many causes, including: motor accidents, falls, gunshot wounds, or diving accidents. Motivated by the need to better understand recovery after SCI, an over-ground, therapeutic robot for research on SCI in rodent models is being developed [3]. Although the device under development targets research on rodents, the ultimate goal is to provide insights on human rehabilitation.

A modular design has been conceived consisting of a robotic device attached to the rat which facilitates movement (Rat Module) and a body weight support system serving to support part or all of the animal's body weight as well as the weight of the Rat Module shown in Fig. 1 [3]. This paper reports the current status of the Body-Weight Support system. A simple system model was developed and verified using experimental data. A passive mechanism to provide partial weight support is also presented. In addition, a closed loop feedback control system was designed and simulated and tested.

2. Overall System Design

2.1. Concept

The therapeutic robot system in [3] consists of three main modules: the movement facilitating device or Rat Module, the Body-Weight Support System (BWSS) which provides partial support to that rat and Rat Module, and the Controller.

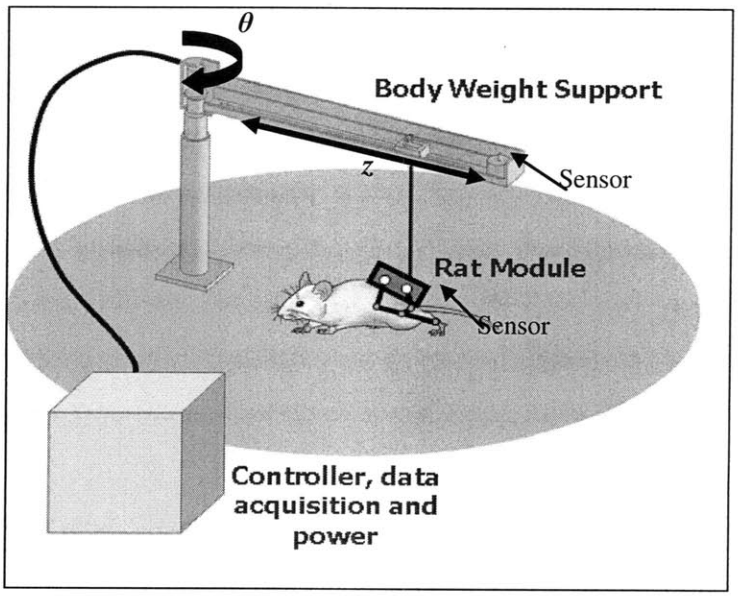

Figure 1: Schematic of a therapeutic robot system which consists of a rat module, body weight support system, and controller. (Courtesy of [3], modified with permission).

The main requirement for the BWSS is to partially support the weight of the injured rat to further facilitate mobility, while allowing unconstrained movement of the rat in the both the radial and circumferential directions as seen in figure 1.

The BWSS was conceived as a crane-like structure which supports the Rat Module vertically by means of a tension element, e.g. a string. The BWSS must allow for unconstrained movement of the rat in both the radial and circumferential directions as seen in Figure 1. This may be achieved by attaching one or more actuators to the body weight structure and using a controller that allows the BWSS to follow the position of the rat.

2.2. Requirements

The body weight support structure must be a system that provides translational and rotational motion allowing for 360 degree rotation and easy access for wires and circuitry. The structure must be able to support at least the weight of the robot module attached to the rat. The rat module is about 43 grams and a rat weighs between 250-400 grams. Sensors must be placed on the rat module and the BWSS to determine the relative position. These sensors must be small and lightweight. The motor used to provide actuation must be provide enough power to rotate a crane arm weighing up to 1 pound and which is about a foot in length. The BWSS must also be a stable, stand alone structure that is relatively lightweight. To ensure stability of the closed looped system, the controller must be able to respond to motions up to 5Hz, which is conceived to be the fastest motion that the injured rat will be able to generate.

Considering the above requirements, it was concluded that a stable pillar structure with a small rotating inertia was the best design for the BWSS. Materials for construction of the BWSS structure were chosen based on availability, cost, weight and machinability as well as strength and durability as per the functional requirements in [3].

2.3. *Design of Structure*

The design of the BWSS structure is shown in Figure 2. The structure consists of two wooden rectangular pillars attached to a crane-arm apparatus. The crane-arm consists of an aluminum rod press-fit inside a plastic disk which is attached to a motor by an aluminum coupling. This design allows for full 360-degree rotation, while permitting easy access for wires and circuitry.

However, the design has a potentially significant drawback of not being able to provide motion in the radial direction. An alternative design was proposed which includes a linear bearing sliding along the aluminum arm for radial movement. It was concluded that with this design, the injured rat might not be able to move the linear bearing in the radial direction given its weight and the friction involved in the materials used.

Although in the current design the radial movement is restricted, the supporting string is still allowed to deviate from vertical, allowing the rat to move within an annulus which would increase the freedom of rat movement. If we allowed 25° deviation from vertical, the width of

the annulus would be 23cm for a 30cm-long string. Nonetheless, if proven to be necessary, the translational degree of freedom may be added in the future.

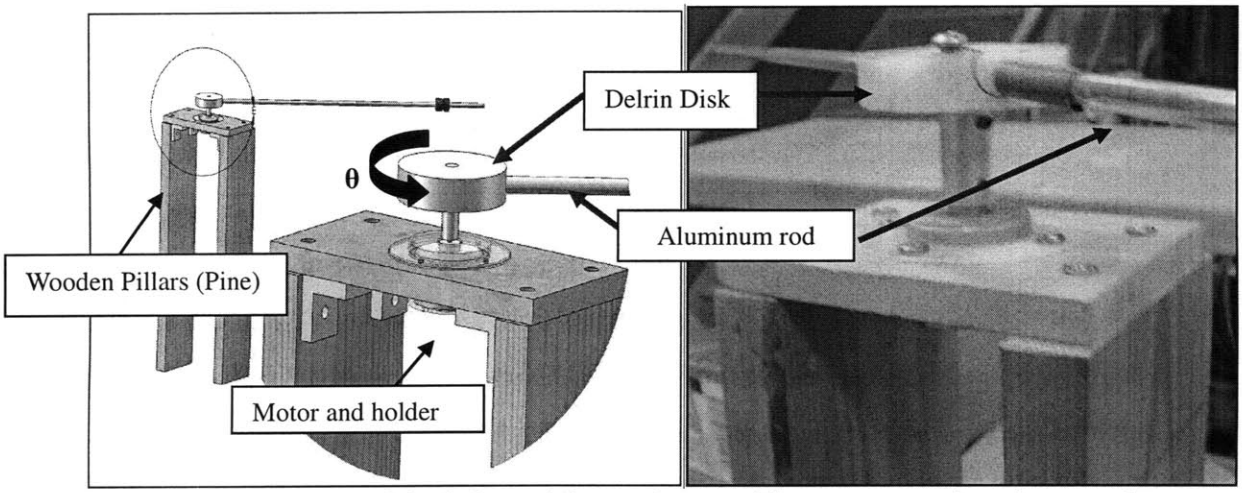

Figure 2: Solidworks drawing of the design and the actual system. The structure consists of two wooden rectangular pillars attached to a crane-arm apparatus. The crane-arm consists of an aluminum rod press-fit inside a plastic disk which is attached to a motor by an aluminum coupling.

2.4. Weight Supporting Mechanism

Figure 3 shows a schematic of the chosen body weight support option which incorporates a spring force to counter the weight of the rat and Rat Module. The inner diameter of the spring is large enough to encircle the aluminum rod of the crane arm. A string is attached to the end of the spring, runs through a hole in the aluminum rod and then is attached to the Rat Module. The friction from the string sliding through the hole in the aluminum rod may be non-negligible, in which case a pulley may be used to minimize this friction. This is deferred to future work.

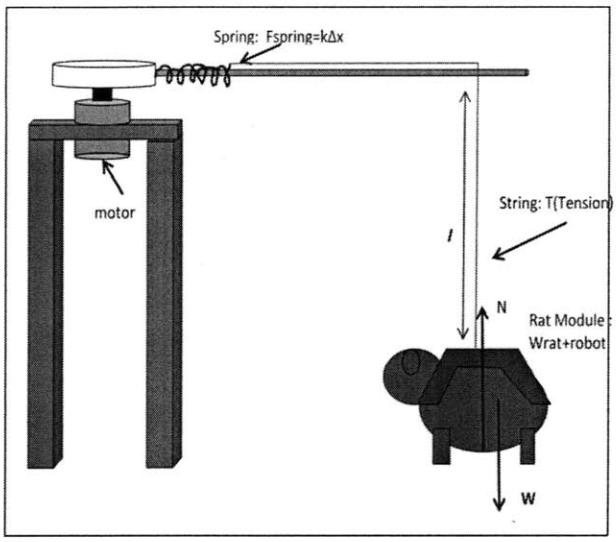

Figure 3: Schematic of the body weight support system. A string is attached to the end of the spring, runs through a hole in the aluminum rod and then is attached to the rat module.

While the rat is weight supported, the contact force *(N)* between the rat and the ground can be written as:

$$N = W - k\Delta x \qquad (1)$$

Consider the instant when the rat has just been attached to the spring in its unloaded state. The rat will travel a distance of Δx before contacting the ground. This distance may be varied by changing l, which is the length of the string between the rod and the Rat Module. We may therefore vary the contact force *(N)* by varying Δx.

Inability to move in the radial direction may also create inaccuracies in force measurements if the string is misaligned from the vertical position. For the model to be accurate, we will assume the force component in vertical direction would not deviate more than 15% which corresponds to a deviation of 0°-25° from vertical.

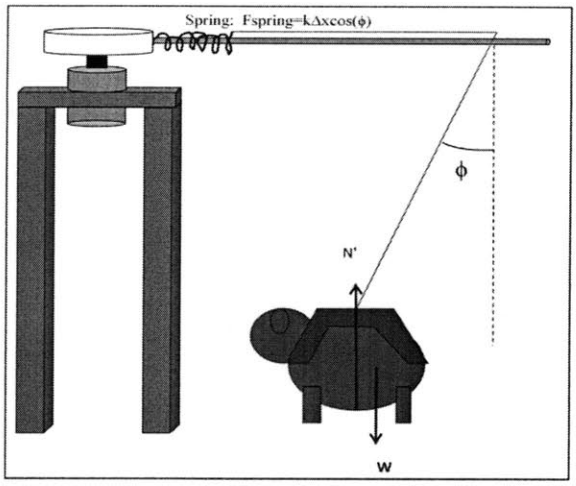

Figure 4: Modified schematic of the body weight support system. The rat is misaligned an angle ϕ from the vertical which causes inaccuracies in force measurements.

Note that for higher spring constants the degree variation must decrease:

$$\%error = \frac{N - N'}{N} = \frac{k\Delta x(1-\cos(\phi))}{W - k\Delta x}$$
$$\Downarrow \qquad (2)$$
$$\phi = \cos^{-1}\left(\frac{\%error \cdot (W - k\Delta x)}{k\Delta x}\right)$$

3. System Model

Figure 2 shows the moving components of the system. Only the rotational degree of freedom is examined (i.e. no movement the radial direction). The equation of motion for the 1 DOF system may be described by the following:

$$\tau = J_{Tot}\alpha_{arm} \qquad (3)$$

Where τ is the actuation torque and α_{arm} angular acceleration of arm. Consider the rotational equation of motion of the system given in equation (3). If we assume that the friction on the motor shaft is proportional to the angular speed of the system. Equation 3 can be written:

$$\tau = J_{TOT}\alpha_{arm} = \tau_i - \tau_f = K_i i - b\omega \qquad (4)$$

Were τ_i is the internal torque of the motor (which is proportional to the motor current), τ_f is the frictional torque, and b is the proportional constant relating angular velocity to friction. By

analyzing motor dynamics (Appendix II), the relation between the input voltage to the motor and the output angular velocity of the crane arm can be obtained:

$$\frac{\Omega(s)}{U(s)} = \frac{1/K_t}{\left[\tau_e\tau_m s^2 + \left(\tau_m + \frac{\tau_e\tau_m}{J}\right)s + \frac{\tau_m b}{J} + 1\right]} \approx \frac{1/K_t}{\left(\tau_m s + \frac{\tau_m b}{J} + 1\right)} \qquad (5)$$

$$where: \quad \tau_m = \frac{RJ}{K_t^2} \quad \tau_e = \frac{L}{R}$$

Here, K_t is the motor constant (N·m/A), R, L, and b are the motor resistance, motor inductance, and damping constants respectively. The mechanical and electrical time constants for the system were computed using the actual values of the parameters to be τ_m =76.5s and τ_e =1.3ms. Since the electrical time constant is much smaller than the mechanical time constant, the dynamics of the electrical system may be neglected, resulting in a first order mechanical system as in (5). Numerical values for Kt and R where determined by several experiments on the motor to determine the torque constant and motor resistance (see Appendix III) . We will attempt to measure the friction constant (b) from experimentation with the actual open loop system as discussed in the following section.

4. Measurement of Steady State Gain

In order to test the feasibility of the model, the open-loop relationship between voltage input and angular speed was measured in steady state by recording the speed of the arm at various applied voltages using an optical tachometer. The current was also notated at the specified voltages to determine the friction constant to be used in the theoretical model calculations.

4.1. *Determination of the Friction Constant*

Assuming constant angular acceleration and linear damping we may find the value for the viscous friction constant friction by the equation:

$$b = \frac{K_t i}{\omega} \qquad (6)$$

Where K_t, i and ω are known values. Figure 5 shows a plot of the ω vs. $K_t i$. From the slope of the trend we may estimate the friction constant to be b = .0005Nm/rad/s. This value is used for

calculation of the gain for the theoretical model. As can be seen, there is a slight curve to the experimental data which suggests the damping is in fact non-linear for the system. However linear damping will be assumed in further calculations since the non-linear trend seems negligible.

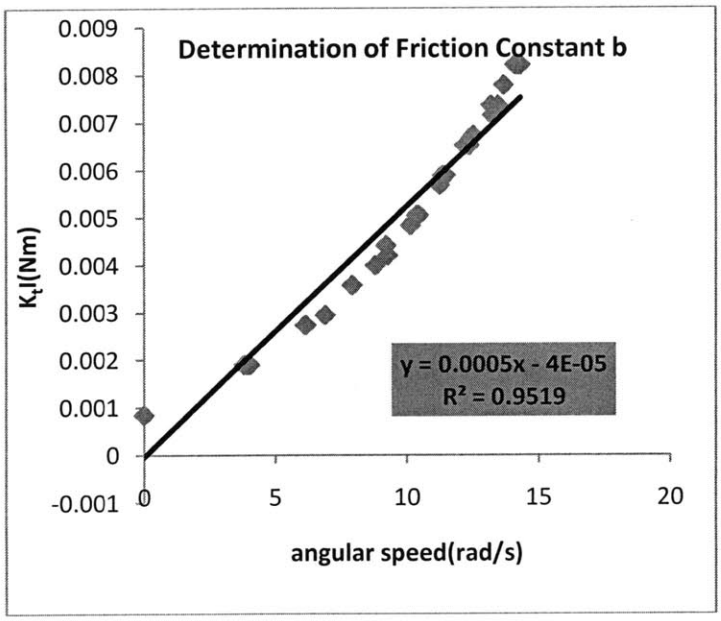

Figure 5: Plot of. K_ti vs. ω. The slope (*b*) is the damping constant value used in determining the steady state gain of the system model.

4.2. *Experimental Results vs Theoretical Model*

The angular speed vs. voltage is plotted in Figure 6. The experimental data was compared against the theoretical system gain determined by equation (5). As can be seen, there is a strong correlation between the experimental data and the theoretical system model with the precision uncertainty value equal to P_{slope}=±.02rad/s. P_{slope} is defined as:

$$P_{slope} = t_{0.025,\nu} \frac{s_{y/x}}{S_{xx}} \tag{7}$$

$$s_{y/x} \equiv \sqrt{\frac{\sum_{i=0}^{n-1} \left(y_i - y(x_i)\right)^2}{n-2}}, \quad S_{xx} \equiv \sqrt{\sum_{i=0}^{n-1} \left(x_i - \bar{x}\right)^2} \tag{8}$$

Where n is the number of data points and $y(x_i)$ is the calculated angular velocity value given by Eq. (5). x_i is the input voltage value corresponding to the measured y_i which is the experimental angular velocity. $\bar{x} \equiv \sum x_i / n$ is the mean x-value of the measurements. σ is the standard and n is the number of measurements.

This quantifies the validity of the mathematical model and justifies its further use to simulate actual system behavior.

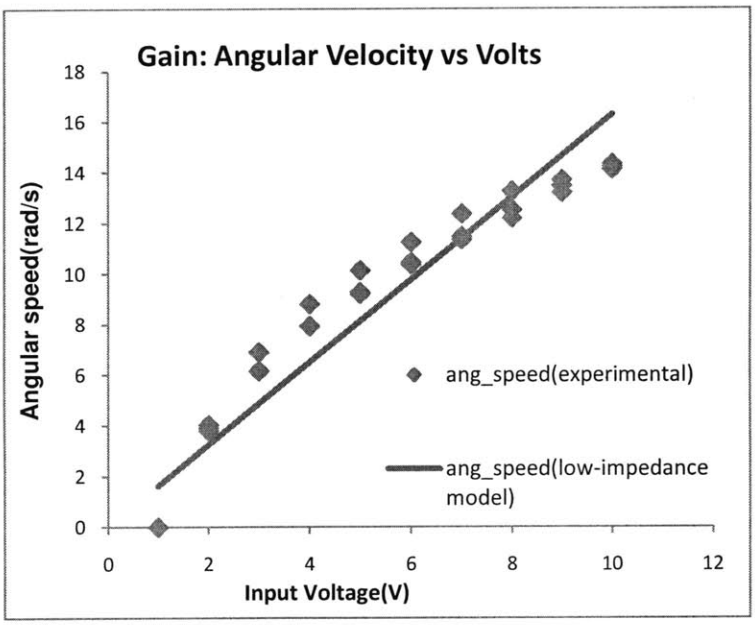

Figure 6: Plot of the experimental angular velocity (rad/s) vs volts(V). The gain determined by the theoretical model (1.63±.020 rad/s/V) shows a strong correlation with the experimental data.

There is also a clear nonlinear trend in the experimental data. The curvature may be due to non-linear damping and/or static friction present in the system.

5. Control System Design

5.1. Accelerometer Signal Processing

To allow the aluminum rod to follow the position of the rat, a closed-loop feedback system with a controller is required. The position of the Rat Module can be monitored by attaching sensors on both the Rat Module and the end of the rod. One option is to use two accelerometers, since the accelerometer signals can be integrated twice to obtain the position. Clearly, integrating twice will introduce substantial drift. Nonetheless, advantages of using accelerometers are that

they are small, lightweight and can be placed in confined spaces. The sensors are simple enough to be used without any external data acquisition system. Also, accelerometers provide practically real-time sensing, as opposed to other possible motion sensors such as the video cameras. The chosen accelerometers output PWM signals, which were averaged using low pass filters as seen in figure 7.

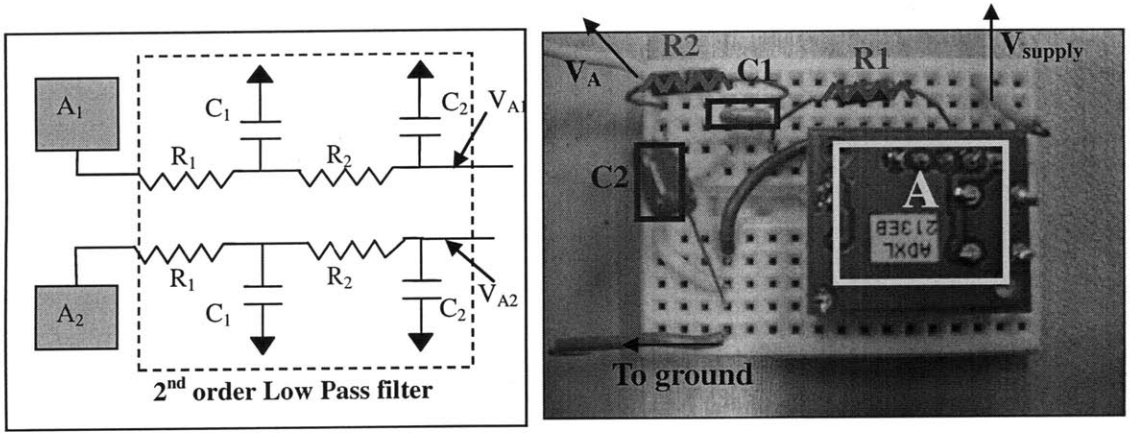

Figure 7: accelerometer circuitry: $A_{1,2}$ –accelerometers, $R_{1,2}$-resitors, $C_{1,2}$-capacitors, V_{A1}-voltage after low pass filtering

5.2. Closed Loop System Simulation

Since the controller is designed to minimize position error between the rat and the BWSS arm, the accelerometers signals must be integrated twice. The integrated accelerometer signals may then be compared and the error signal inputted into the controller. A block diagram depicting the closed loop system is shown in figure 8.

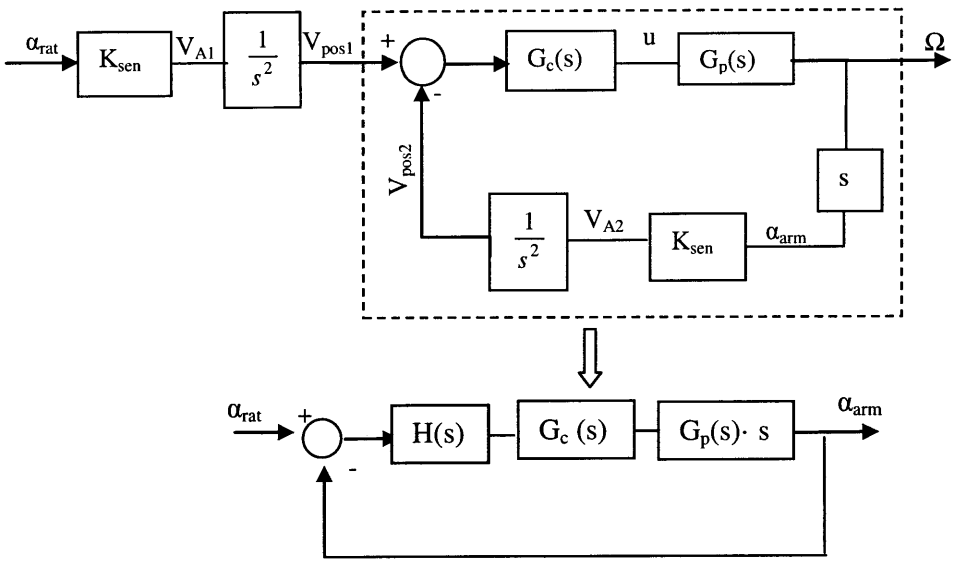

Figure 8: Block diagram of closed loop control system. The integrated accelerometer signals are compared and the error signal inputted into the controller.

Proportional derivative (PD) control was chosen for the controller because it was concluded to be sufficient to control position error. Integral action (as in PID control) is unnecessary and may even complicate the system since the system already contained two integrators. $G_c(s)$ is the transfer function for the PD controller given by the equation:

$$G_c(s) = K_D(s+a) \quad where\ a = \frac{K_p}{K_D} \tag{9}$$

The sensor dynamics can be described by equation:

$$H(s) = \frac{K_{sen}}{s^2} \tag{10}$$

Where K_{sen} is the sensor gain and the s^2 in the denominator signifies the double integration needed to change the accelerometer signal to a position signal. $G_p(s)$ is the open loop system described by (5).

Figure 9 shows the Bode diagram for the closed loop system where the collective gain $G = K_{sen}K_tK_d = 10\frac{N \cdot m}{A} \times \frac{V \cdot s}{rad}$ was chosen such that the damping coefficient is ζ=.7, which is the conventional value used in control system design. The controller zero, $a=K_P/K_D=50$, was chosen to in order to ensure correct placement of closed-loop poles and set the magnitude of the DC gain to ensure stability.

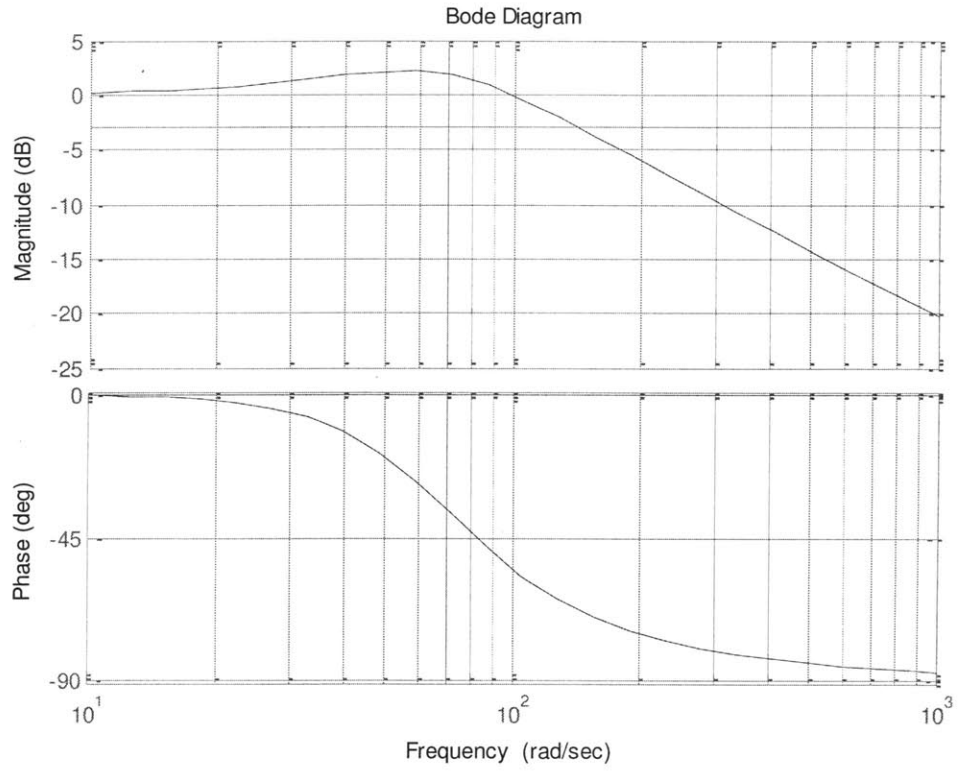

Figure 9: Bode diagram of the closed loop system $Gcl = \left(\frac{\alpha_{arm}}{\alpha_{rat}} \right)$ of fig. 5. G = 10(Nm/A)·(V/rad/s), a=K_p/K_d= 50, ζ=.7

As can be seen from the Bode plot the bandwidth is 141.5 rad/sec (22.5 Hz) which is sufficient to accommodate the inputs to the system since the injured rat will be unlikely to generate movement over 5 HZ.

5.3. *Analog Circuitry*

The controller circuit consists of a double integrator (which converts acceleration error signal to a position signal), and a PD controller as shown below in figure 10.

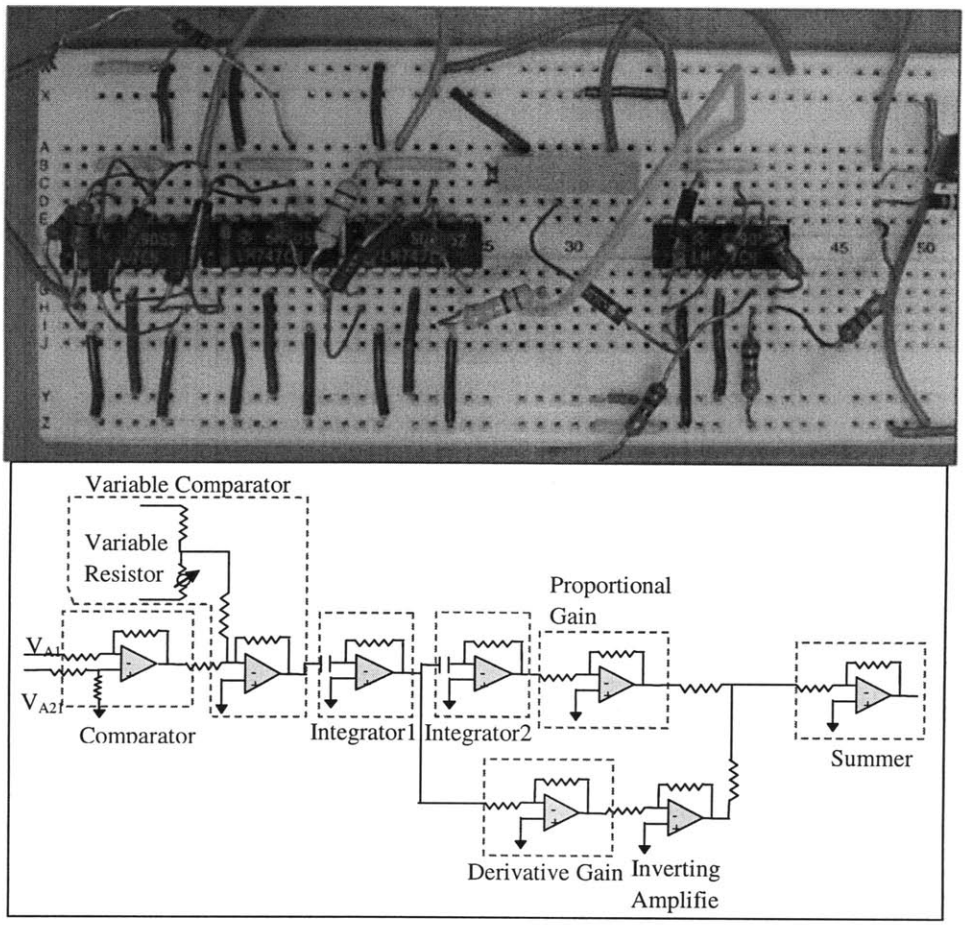

Figure 10: Controller circuitry consists of double integrator (which converts acceleration error signal to a position signal), and a PD controller.

As can be seen in figure 10, an analog comparator consisting of an op-amp and resistors was used to obtain the error in acceleration. However, due to variations in accelerometer offsets, the error signal is not exactly zero when both accelerometers are aligned and at rest. Because of this, there is a significant drift when the signal is integrated. In attempt to resolve the offset issue, a variable comparator consisting of a variable resistor was designed to allow the error signal be set to a zero value manually. However due to inherent inaccuracies in the analog systems, the bias could not be removed with sufficient accuracy to be functional for the intended application. The following sections discuss alternate methods of control.

6. Alternate Methods of Control

6.1. *Analog Design using High Pass filter*

A high pass filter may be added after the comparator to completely eliminate the DC offset and only pass signals with varying frequency (Figure 11). Although this method would eliminate the drift caused by integration, the system would not respond to very slow motion which is a required function since the injured rat will be moving at a slow pace.

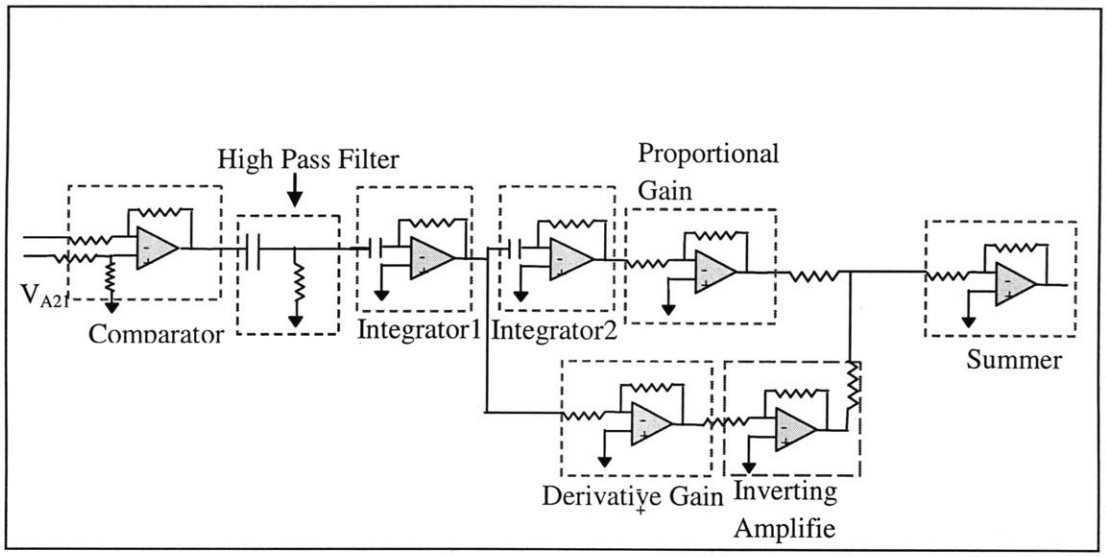

Figure 11: Revised controller circuitry. A high pass filter may be added after the comparator to completely eliminate the DC offset.

7.2 Using Digital Systems and Numerical Integration

The comparator and controller operations may be conducted with increased precision with the aid of a computer and using a simple C program (see Appendix VI). To approximate the position and velocity we may consider the Newton Euler method:

$$\omega_{i+1} = \omega_i + \alpha_i \Delta t \qquad (11)$$

$$\theta_{i+1} = \theta_i + \omega_i \Delta t \qquad (12)$$

$$i = 0,1,2...$$

Where $\Delta t = \dfrac{1}{sampling\ frequency}$. These calculations approximate the position and velocity considering the first term of a Taylor series expansion.

The acceleration signal is converted from voltage following the equation:

$$acceleration = K_{sen} \cdot (V_{LPF} - .5 \cdot V_{supply})$$
$$where: K_{sen} = \frac{3.33}{V_{supply}} \cdot 9.8 \frac{m}{s^2} \quad (13)$$

Here, the bias is 50% of the supply voltage. Since the supply voltage is not nominally known, the acceleration is still offset at rest. Because of this variation, unnecessary integration is still occurring and the sensor gain is inaccurate. To counter this problem, the initial two seconds of the accelerometer signal (when the accelerometer is at rest) is averaged and stored as the bias value. This average signal is also used to calculate the voltage supply to obtain a more accurate sensor gain:

$$acceleration = K_{sen} \cdot (V_{LPF} - V_{LPF,initail})$$
$$where: K_{sen} = \frac{3.33}{2 * V_{LPF,initial}} \cdot 9.8 \frac{m}{s} \quad (14)$$

With these corrections, the controller appeared to be functional and the correct response was observed from the BWSS. A qualitative experiment was conducted to observe the response of the system by attaching the control voltage output from the computer to the BWSS system as shown in figure 12.

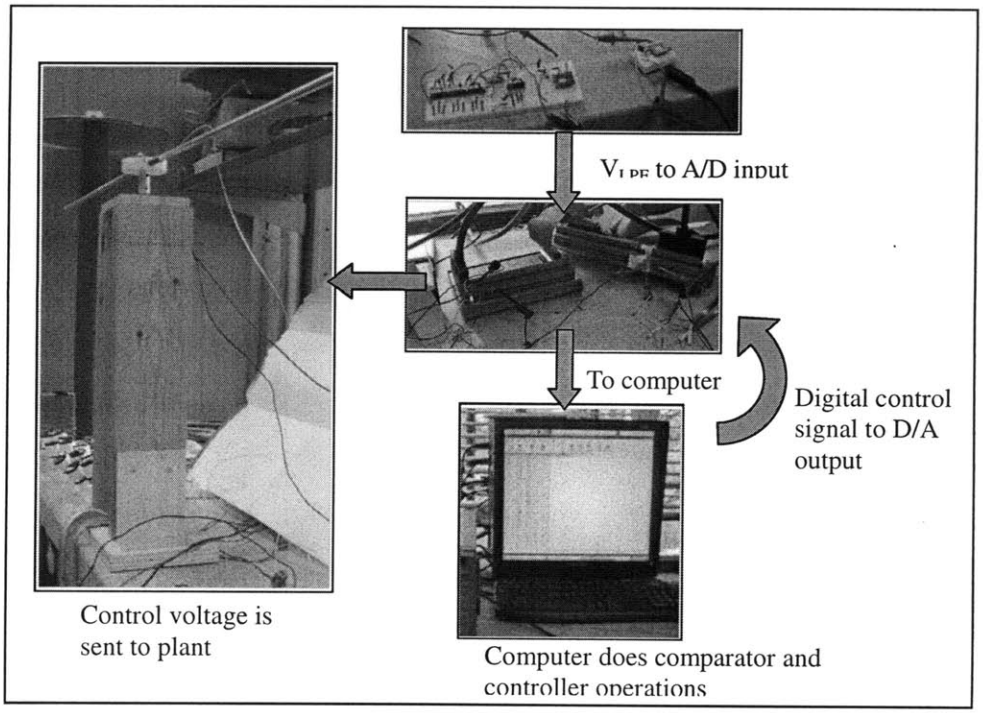

Figure 12: Schematic of preliminary test to assess qualitative behavior.

It was observed that when a constant error was introduced between the accelerometers (mimicking a situation in which the rat is accelerating in a manner to keep a constant distance from the crane arm) the crane arm accelerated in an attempt to minimize the error. Furthermore, when the error between the accelerometers was decreased (mimicking a situation in which the rat is slowing down) the crane arm began to decelerate and stopped when the accelerometers where aligned. More accurate and quantitative assessment of the system is deferred for future work.

Discussion

Although it was shown that there is a strong correlation between the open loop dynamics and the system model, more analysis must be completed before the closed loop system model may be considered valid. This cannot be done presently because to obtain accurate position data a position shaft encoder should be integrated into the design of the BWSS. Also at present the inertia of the crane arm is too large for the current motor and a larger motor is needed. Also the voltage limit on the computer is ±10 volts which is not enough to accommodate the dynamic response of the system. Because of this, the system saturates before it has a chance correctly respond. These factors were not anticipated at the start of the project. However, the system responds as intended a shown in the previous section. These corrections would be done to quantify the accuracy of the response to the simulated closed loop system

Also, it can be deduced that the most reliable and practical method for control is through the computer. This method of control should be used and incorporated in future analysis and design. However, if a computer is used there is inevitably a delay due to sampling. Considering that our system is intended for slow movements, time delay is a non-issue.

Conclusion

The goal of this on-going project is to develop a highly back-drivable robotic therapeutic device for studies of recovery in SCI in rodent models. A body weight support system prototype was developed and its open loop dynamics analyzed. An open loop system model was compared with experimental data. A strong correlation was found between the open loop system model gain and the experimental gain. A controller simulation based on the model was created to verify the feasibility of the closed loop system. Appropriate values for proportional, derivative, steady state gain were determined from the simulation. After the intended method of obtaining closed

loop feedback control using analog circuits was concluded to be impractical, other methods of control were explored. The method of numerical integration using the computer was shown to be valid. Future work should include integrating the controller circuitry with the BWSS design and obtaining experimental data to verify the closed loop system.

Acknowledgements

Supported in part by The Eric P. and Evelyn E. Newman Laboratory for Biomechanics and Human Rehabilitation. Special thanks to Yun Seong Song my direct supervisor.

References

[1] Nessler JA, Timoszyk W, Merlo M, Emken JL, Minakata K, Roland RR, "A Robotic Device for Studying Rodent Locomotion after Spinal Cord Injury." *IEEE Transactions on Neural Systems and Rehabilitation Engineering* 13(4), 2005, pp. 497-506

[2] Jezernik S, Colombo G, Keller T, Frueh H, Morari M, "Robotic Orthosis Lokomat: A Rehabilitation and Research Tool." *Neuromodulation* 6(2), 2003, pp. 108–115.

[3] Song YS, Hogan N, 2008 "Design Of An Overground Interactive Therapeutic Robot For Rodents Recovering After Spinal Cord Injury". *Proceedings of ASME Dynamic Systems and Control Conference,* 2008, pp. 409-411.

[4] Krebs HI, Volpe BT, Williams D, Celestino J, Charles SK, Lynch D, Hogan N, "Robot-Aided Neurorehabilitation: A Robot for Wrist Rehabilitation." *IEEE Transactions on Neural Systems and Rehabilitation Engineering* 15(3), 2007, pp.327–335.

[5] Kwakkel G, Kollen BJ, Krebs HI. "Effects of Robot-Assisted Therapy on Upper Limb Recovery after Stroke: A Systematic Review," *Neurorehabilitation and Neural Repair* 22(2), 2007, pp.111-121.

[6] Roy A, Krebs HI, Williams DJ, Bever CT, Forrester LW, Macko RM, Hogan N, "Robot-Aided Neurorehabilitation: A Novel Robot for Ankle Rehabilitation." *IEEE Transactions on Robotics*, 25(3), 2009, pp.569-582.

Appendix I

Part Drawings

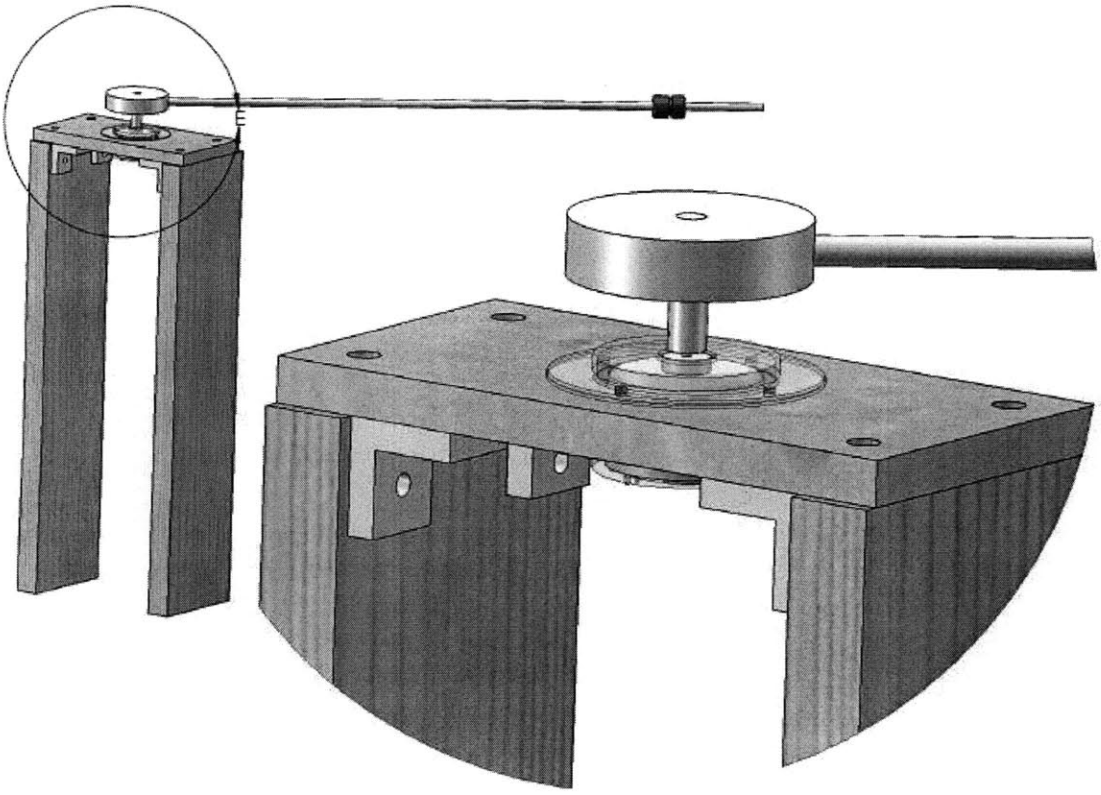

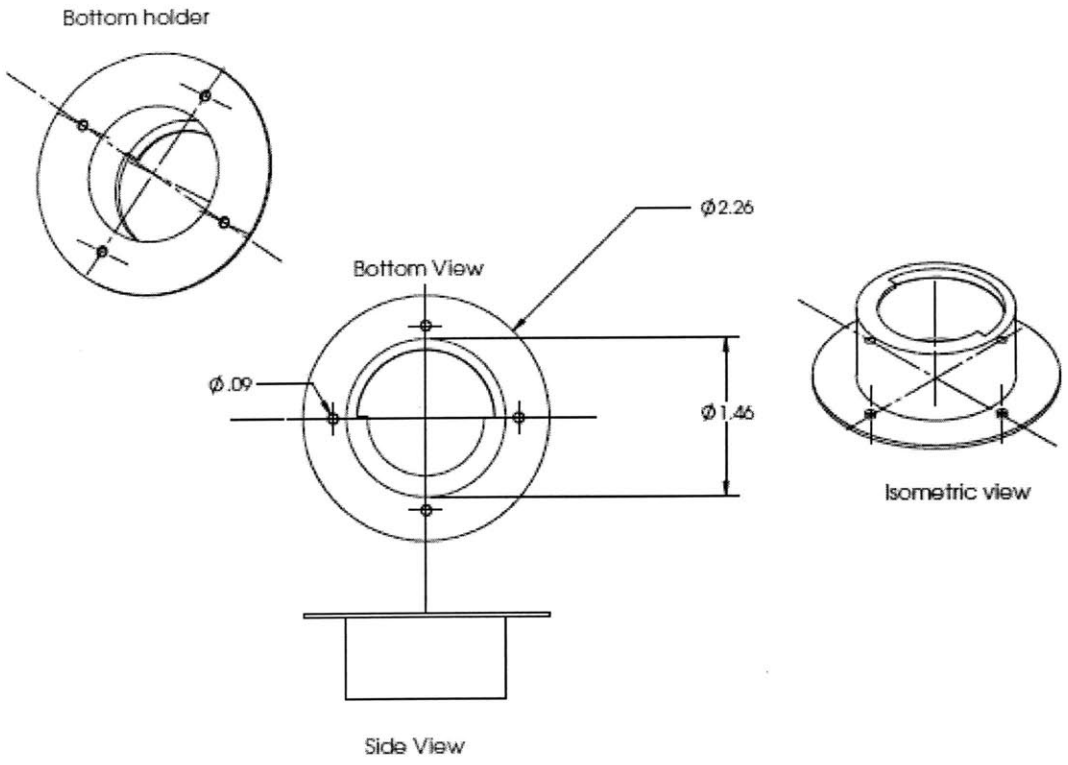
Bottom holder
Bottom View
Ø2.26
Ø.09
Ø1.46
Isometric view
Side View

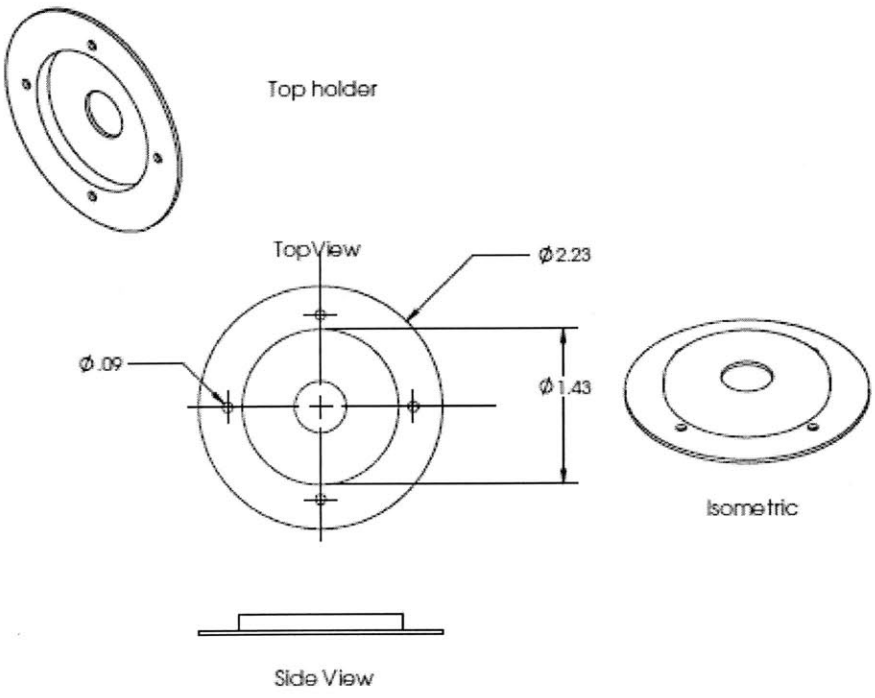
Top holder
TopView
Ø2.23
Ø.09
Ø1.43
Isometric
Side View

Wheel(Delrin)

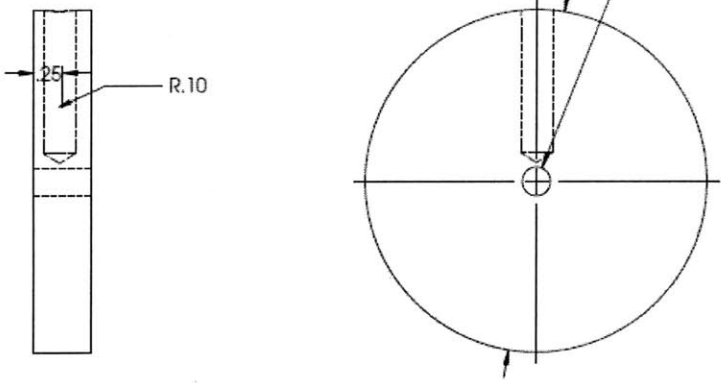

Motor Coupling(Delrin)

Step	Task	Tool
1	Cut stock to specified diameter	lathe
2	Drill 1/4" diameter bottom whole	lathe
3	Drill 2mm diameter top whole	lathe
4	Drill 1mm(side wholes)	mill

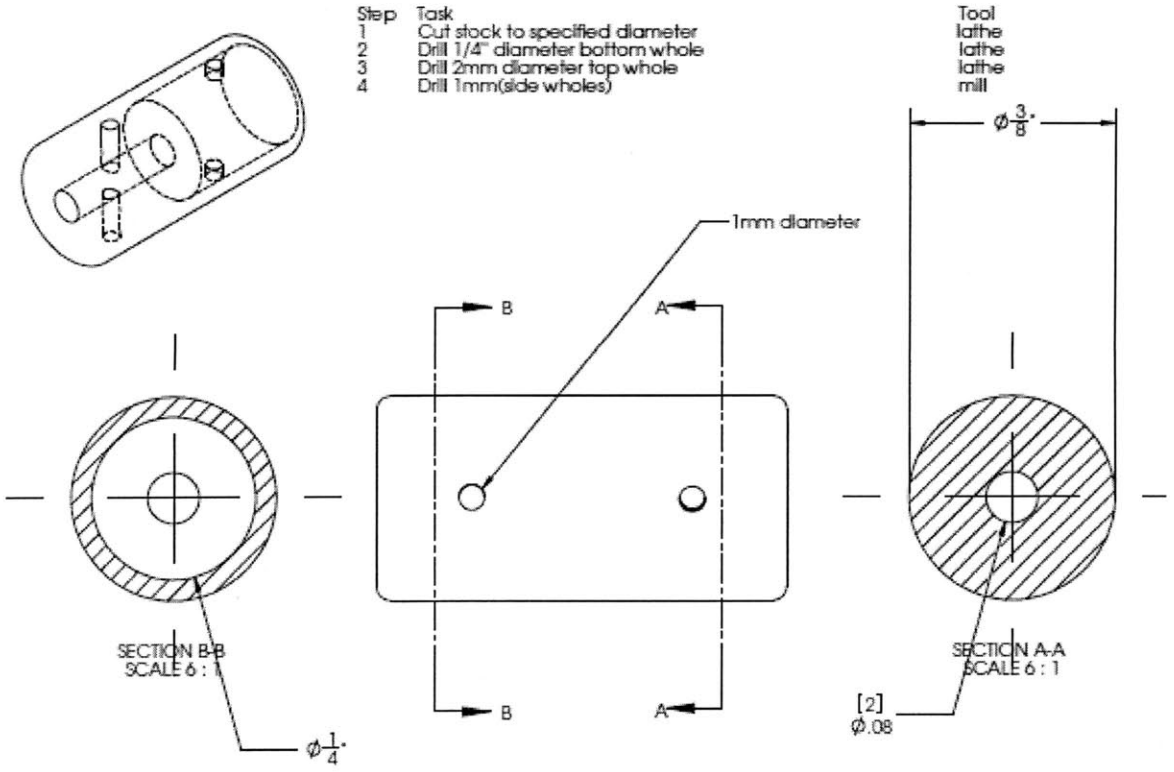

Appendix II

System Model Calculations

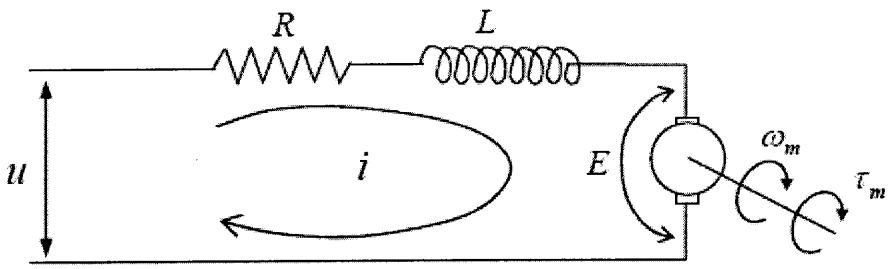

$$u = R \cdot i + L\left(\frac{d}{dt} i\right) + E(\omega) \qquad (1)$$

The EMF voltage is in general proportional to the angular velocity, and is given by:

$E = K_t \cdot \omega_m$ (2)

where the proportionality constant $\mathbf{K_t}$ is called the torque constant.

We may rewrite the differential equation as:

$$u = R \cdot i + L\left(\frac{d}{dt} i\right) + K_t \cdot \omega_m \qquad (3)$$

Taking the Laplace Transform, we obtain:

$$U(s) = R \cdot I(s) + L \cdot s \cdot I(s) + K_t \cdot \Omega_m(s) \qquad (4)$$

Torque can be expressed as:

$$\tau_s = \tau = [I_1 + I_2 + m_2 z^2]\, \theta'' = [I_1 + I_2 + m_2 z^2]\, \omega_m \qquad (5)$$

let us substitute $[I_1 + I_2 + m_2 z^2]$ with J_{TOT}

Taking the Laplace, we obtain:

$$T_s(s) = J_{TOT} \cdot s \cdot \Omega_m(s) \qquad (6)$$

The *internal* armature torque is in general proportional to current by the equation:

$$\tau_i = K_t \cdot i \qquad (7)$$

Because of friction, the shaft torque τ_s is less than the internal torque:

$$\tau_s = \tau_i - \tau_f = K_t i - b\omega \qquad (8)$$

Where τ_f is the torque due to friction which is proportional to the angular velocity with proportionality constant b.

We may now use equations 6 and 8 to solve for $\mathbf{\Omega_m(s)}$:

$$\mathbf{\Omega_m(s)} = \frac{K_t I(s)}{Js + b} \qquad (9)$$

Substituting $\Omega_m(s)$ into equation 4 we obtain:

$$U(s) = (R + Ls + \frac{K_t^{\,2}}{J_{TOT}s + b})I(s) \qquad \textbf{(10)}$$

Using current torque proportionality:

$$\mathbf{U(s)} = \left(\frac{R}{K_t} + \frac{L}{K_t}s + \frac{K_t}{J_{Tot}\cdot s + b}\right)[T(s) + b\Omega(s)] \qquad \textbf{(11)}$$

Since $\tau = J_{ToT}\alpha = J_{ToT}s\Omega(s)$

$$\mathrm{U(s)} = \left(\frac{(R + Ls)(Js + b) + K_t^{\,2}}{K_t}\right)\Omega(s) \qquad \textbf{(12)}$$

Therefore the Plant/Motor transfer function can be written:

$$\mathrm{Gp(s)} = \frac{\Omega(s)}{U(s)} = \frac{K_t}{(R + Ls)(J_{Tot}s + b) + K_t^2} \qquad (13)$$

If we assume that the inductance is small, this equation may be further reduced to a first order system:

$$\boxed{G_p(s) = \frac{K_t}{\left(J_{ToT}R\cdot s + bR + K_t^2\right)}}$$

The transfer function for angular velocity is(first order):

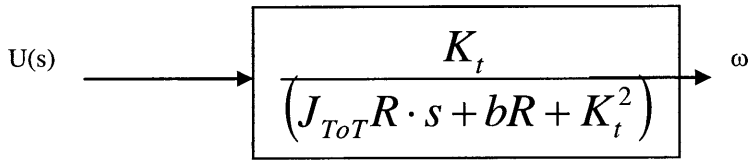

Appendix III

Determination of Motor Characteristics

Determination of Torque Constant

Since the DC motors ordered did not come with specs, I performed several experiments on the motor to determine the torque constant and motor resistance. Below I have outlined the experimental apparatus and procedure.

Apparatus:

Below is the schematic for the experiment:

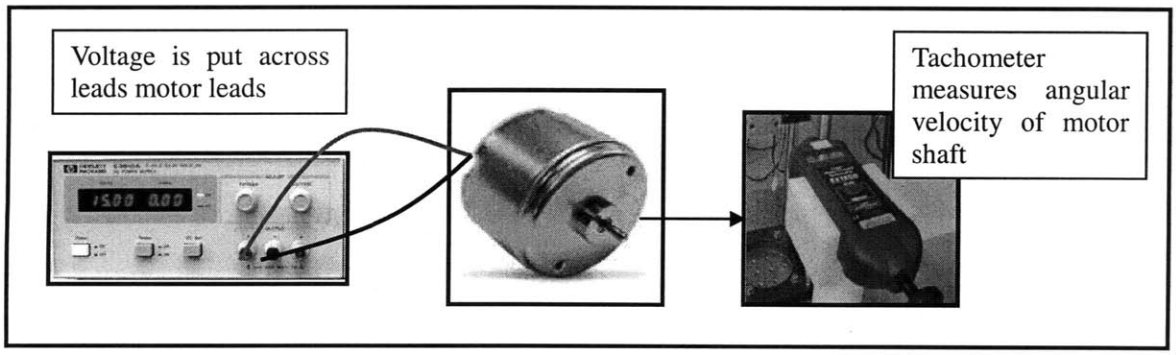

Apparatus Elements:

1. Motor
2. holder
3. black and white disk
4. tachometer
5. Wires

Experimental Procedure:

1. Attach the motor leads to power supply(voltage source) with wires
2. Measure the rotational speed with the tachometer measures in RPM) for 0 – 12 V in steps of 2 V.
3. Plot angular velocity, Ω (in radian/sec) vs. V and use a best-fit line to determine Ke (the inverse of the slope)

Determination of Armature Resistance

The determination of armature resistance was determined by the following procedure:

Apparatus:

Below is the apparatus for the experiment:

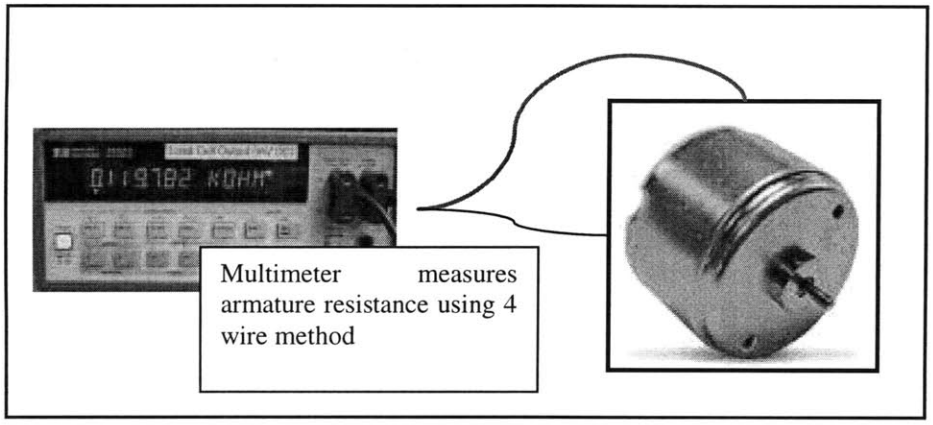

Apparatus elements:

1. Motor
2. Multimeter
3. mini-clip to BNC adapter
4. banana to BNC cable

Procedure:

1. Connect Motor to Multimeter using mini-clip to BNC adapter and banana to BNC cable.
2. Measure armature resistance using Multimeter.

Appendix IV

Open Loop System Experimentation

Preliminary System Identification Experiment

The following experiment was conducted to obtain a preliminary system identification of the BWSS system. By performing a system ID we may ensure stable control in the future. Since an optical encoder was not available, an optical tachometer was used to study the open loop relationship between voltage input and angular velocity.

Experimental Apparatus

Experimental Apparatus Elements:

1) AUTOTROL-052-0010AD DC Brush Motor
2) Function Generator/Computer/Power Supply
3) Voltage Power supply
4) BWSS Structure
5) EXTECH Tachometer(Range: 10 to 99,999 rpm)
6) BNC Cables
7) BNC to mini-clip adapters
8) Ring Stand

Schematic of Experimental Apparatus:

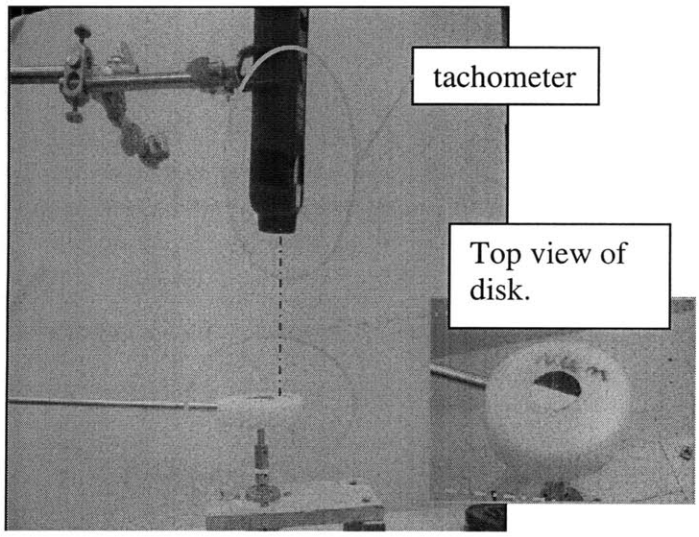

Figure 13: Picture of the experimental setup. The tachometer responds to the light and dark patches on the disk. A voltage source was connected to the motor leads

Experimental Procedure

After setting up the apparatus as shown, the BNC cable terminated in mini-clips was connected between the motor terminals and the Power supply. The voltage was set to the initial value of 1V and the RPM was read from the tachometer LCD and recorded. The angular speed was recorded for 1-12V. The experiment was then repeated with the initial voltage 12V and decreased to 1 V.

Appendix V

Controller Simulation

```
%%%%Plant parameters

% Calculate Moment of inertia
D = 0.0508; %m
Dr = 0.00635; %m
t = 0.0127; %meters
l = 0.4572; %meters
Ad = pi*D^2/4; %m^2
Ar = pi*Dr^2/4; %m^2
Vd = Ad*t; %m^3
Vl = Ar*l; %m^3
rhod = 1383.99524; %kg/m^3(delrin density)
rhoa = 2823.35028; %kg/m3(aluminum density)
md = rhod*Vd;    %kg
ml = rhoa*Vl;    %kg
Jd = .5*md*(D/2)^2; %m^2*kg
Jlr = (1/3)*ml*l^2; %m^2*kg
Jc = 3.577e-8; %m^2*kg
Jsr = 1.717e-7; %m^2*kg

%Parameters
Kt = .02;  %Vs/rad
R = 18.18; %Ohms
b = .0005; %Nms
J = Jd + 2*Jlr+ Jc + Jsr; %m^2*kg

%%%%Plant Tranfer function
num1 = [1 0];     %Numerator: Kts
den1 = [J*R b*R+Kt^2];    % Denominator: JRs + bR + Kt^2

Gp = tf(num1,den1);

% %Feedback with SensorPD control: kd(s+kp/kd)
s = tf('s');
Vs = 4; %V
Ksen = (Vs/(3.33*9.8)); %Vs/(m/s) sensor gain
I = tf([1],[1 0 0]); % integrator
H =I;
Kcol = 1;  %Kcol = kd*Ksen*kt colective gain
hold on
for a = 50; % kp/kd is a set value
C = (s+a); %a = kp/kd is a set value
Gf = Kcol*H*C*Gp;
Gcl = feedback(Gf,1);
pole(Gcl);
zero(Gcl);
rlocus(Gf)
% bode(Gf)
end
grid
```

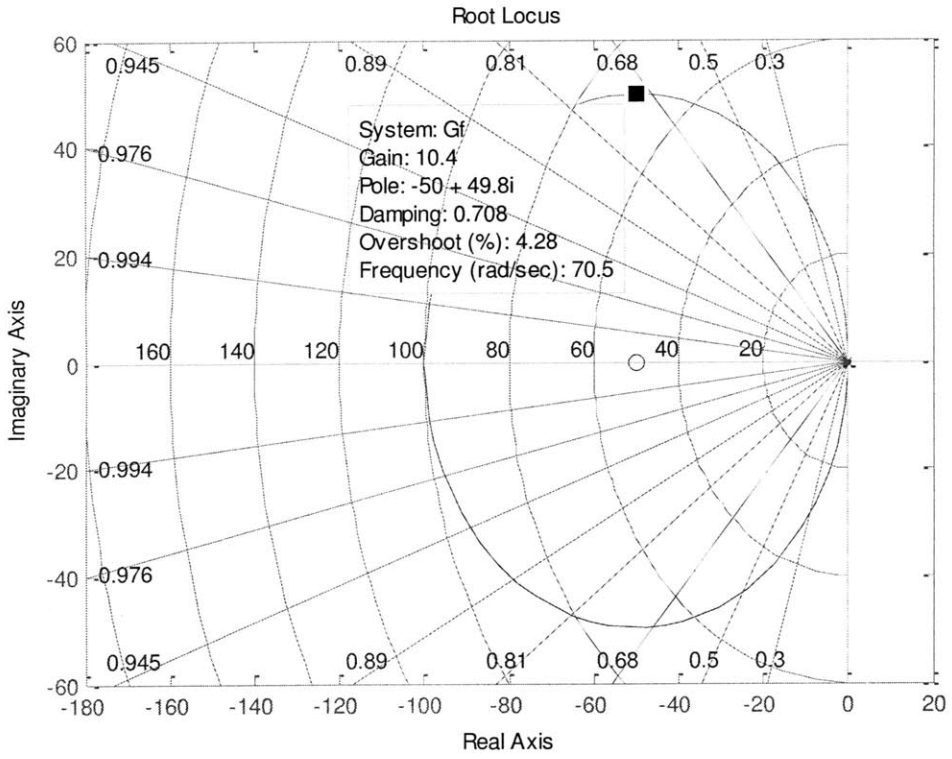

FIGURE 14: ROOT LOCUS OF CLOSED LOOP SYSTEM $\mathbf{Gcl} = \left(\frac{\boldsymbol{\alpha}_{\mathbf{arm}}}{\boldsymbol{\alpha}_{\mathbf{rat}}} \right)$ G = 10, A=K_P/K_D= 50

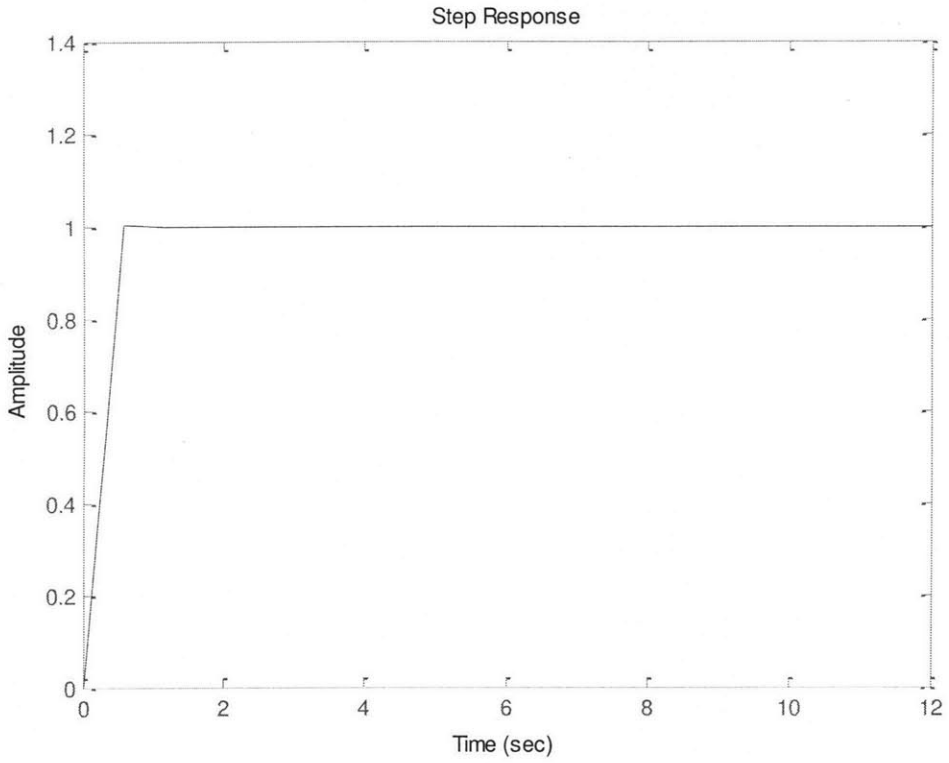

FIGURE 15: STEP RESPONSE OF CLOSED LOOP SYSTEM $\mathbf{Gcl} = \left(\frac{\boldsymbol{\alpha}_{\mathbf{arm}}}{\boldsymbol{\alpha}_{\mathbf{rat}}} \right)$ G = 10, A=K_P/K_D= 50

Appendix VI

Numerical Integration Code

```
// This code is for Michaelle's Senior Thesis Project. Written
04/20/2010 by Yun Seong Song
// Takes two voltage input from two LPF'ed accelerometers, integrates
them to position and then
// outputs the PD-controlled voltage.
void
BWSS(void)
{
  f64 accel1, accel2;
  f64 delta_t;
  f64 sup_volt1, sup_volt2;
  f64 sensor_gain1, sensor_gain2;
  f64 P_gain, D_gain;
  f64 offset1, offset2;

  // PARAMETER INITIALLIZATION
  //sup_volt1 = 4.0;  // supply voltage into the first accelerometer.
  //sup_volt2 = 4.0;  // supply voltage to the second accelerometer.
Can be different from sup_volt1.
  delta_t = 1.0 / ob->Hz;  // One sampling time = 1/freq
  //sensor_gain1 = 5.0 / 3.0 * 2.0 / sup_volt1 * 9.8; // 5/3 (g) * 2
(direction) / (supply voltage) * 9.8 (m/s^2/g)
  //sensor_gain2 = 5.0 / 3.0 * 2.0 / sup_volt2 * 9.8; // same as
above.
  P_gain = 6000;  // Proportional gain on POS error. Adjust
accordingly.
  D_gain = 600;  // Derivative gain on POS error = Proportional gain
on VEL error. Adjust accordingly.

  // rob->rat.misc.front_amp is for the first accelerometer's reading
at zero acceleration (offset voltage)
  // rob->rat.misc.rear_amp is for the second one.
  // These are measured automatically during the first 3 or so
seconds.
  offset1 = rob->rat.misc.front_amp;
  offset2 = rob->rat.misc.rear_amp;

  if (ob->i < 2 * ob->Hz)
  {
      rob->rat.misc.front_amp = rob->rat.misc.front_amp + daq-
>m_adcvolts[1][1];
      rob->rat.misc.rear_amp = rob->rat.misc.rear_amp + daq-
>m_adcvolts[1][2];
  }
  else if(ob->i == 2 * ob->Hz)
  {
      rob->rat.misc.front_amp = rob->rat.misc.front_amp / (2 * ob->Hz);
      rob->rat.misc.rear_amp = rob->rat.misc.rear_amp / (2 * ob->Hz);

      sup_volt1 = 2.0 * rob->rat.misc.front_amp;
```

```
      sup_volt2 = 2.0 * rob->rat.misc.rear_amp;

      sensor_gain1 = 5.0 / 3.0 * 2.0 / sup_volt1 * 9.8; // 5/3 (g) * 2
(direction) / (supply voltage) * 9.8 (m/s^2/g)
      sensor_gain2 = 5.0 / 3.0 * 2.0 / sup_volt2 * 9.8; // same as
above.

      rob->rat.PID.rear_right.error = sensor_gain1;
      rob->rat.PID.rear_right.summed_error = sensor_gain2;
   }
   else
   {
      offset1 = rob->rat.misc.front_amp;
      offset2 = rob->rat.misc.rear_amp;
         sensor_gain1 = rob->rat.PID.rear_right.error;
      sensor_gain2 = rob->rat.PID.rear_right.summed_error;
        // READ SENSORS
        accel1 = ( daq->m_adcvolts[1][1] - offset1 ) * sensor_gain1; //
acceleration, unit = m/s^2
        accel2 = ( daq->m_adcvolts[1][2] - offset2 ) * sensor_gain2; //
same as above.

        // CONTROLLER ACTION
        // rob->rat.PID.rear_left.error  -- means acceleration error
        // rob->rat.PID.front_left.error -- means veloccity error
        // rob->rat.PID.front_right.error-- means position error
        rob->rat.PID.rear_left.error = (accel1 - accel2);  // error in
acceleration, unit = m/s^2
        // first integrator, unit = m/s
        rob->rat.PID.front_left.error = rob->rat.PID.front_left.error +
rob->rat.PID.rear_left.error * delta_t;
        // second integrator, unit = m
        rob->rat.PID.front_right.error = rob->rat.PID.front_right.error
+ rob->rat.PID.front_left.error * delta_t;

        // OUTPUT
        // outputs the PD_controlled voltage to channel zero.
        MOTOR2 = P_gain * rob->rat.PID.front_right.error + D_gain *
rob->rat.PID.front_left.error;
   }
}
```